doi:10.1111/evo.14272

Selection and isolation define a heterogeneous divergence landscape between hybridizing *Heliconius* butterflies

Steven M. Van Belleghem,[1,2] Jared M. Cole,[3,4] Gabriela Montejo-Kovacevich,[5] Caroline N. Bacquet,[6] W. Owen McMillan,[7] Riccardo Papa,[1,8] and Brian A. Counterman[3,9,10]

[1]*Department of Biology, University of Puerto Rico, Rio Piedras, Puerto Rico*

[2]*E-mail: Steven.Van@upr.edu*

[3]*Department of Biological Sciences, Mississippi State University, Mississippi State, USA*

[4]*Department of Integrative Biology, University of Texas at Austin, Austin, Texas, USA*

[5]*Department of Zoology, University of Cambridge, Cambridge, UK*

[6]*Universidad Regional Amazonica Ikiam, Tena, Ecuador*

[7]*Smithsonian Tropical Research Institute, Panamá, Panama*

[8]*Molecular Sciences and Research Center, University of Puerto Rico, San Juan, PR*

[9]*Department of Biological Sciences, Auburn University, Alabama, USA*

[10]*E-mail: bac0071@auburn.edu*

Received May 7, 2020
Accepted May 12, 2021

Hybridizing species provide a powerful system to identify the processes that shape genomic variation and maintain species boundaries. However, complex histories of isolation, gene flow, and selection often generate heterogeneous genomic landscapes of divergence that complicate reconstruction of the speciation history. Here, we explore patterns of divergence to reconstruct recent speciation in the erato clade of *Heliconius* butterflies. We focus on the genomic landscape of divergence across three contact zones of the species *H. erato* and *H. himera*. We show that these hybridizing species have an intermediate level of divergence in the erato clade, which fits with their incomplete levels of reproductive isolation. Using demographic modeling and the relationship between admixture and divergence with recombination rate variation, we reconstruct histories of gene flow, selection, and demographic change that explain the observed patterns of genomic divergence. We find that periods of isolation and selection within populations, followed by secondary contact with asymmetrical gene flow are key factors in shaping the heterogeneous genomic landscapes. Collectively, these results highlight the effectiveness of demographic modeling and recombination rate estimates to disentangling the distinct contributions of gene flow and selection to patterns of genomic divergence.

KEY WORDS: Admixture, heterogeneous divergence, reproductive isolation, selection, species boundaries.

Disentangling the factors that drive genomic divergence is necessary for advancing our understanding of speciation. Targets of selection, for example, may be responsible for adaptive differences between species and their number, distribution, and effect on gene flow along the genome define the architecture of species boundaries. In population genomic studies, targets of selection are expected to show elevated divergence between species (Wolf and Ellegren 2017). These highly divergent loci often reflect local adaptation and/or incompatibilities between species, and can be considered the loci that define the species (Wu 2001; Ravinet et al. 2017). Natural selection thus acts to produce local genomic "barriers" to gene flow between hybridizing species (Arias et al.

2016; Tavares et al. 2018; Edelman et al. 2019; Martin et al. 2019). In contrast, the rest of the genome, which is not under such selective pressures, is often expected to be exchanged more freely between the species (i.e., gene flow). However, genetic variation at these latter genomic regions can be greatly influenced by neutral demographic processes (i.e., population size and migration) and the indirect effects of nearby targets of selection. Local recombination rates can further influence the extent to which selection impacts these nearby targets of selection or linked genetic variation, which collectively results in highly heterogeneous patterns of divergence (Charlesworth 2009; Aeschbacher et al. 2017; Burri 2017; Wolf and Ellegren 2017; Martin et al. 2019; Stankowski et al. 2019). Thus, to make correct inferences about the contribution of selection to the evolution of barrier loci, it is important to consider all processes that can shape the genomic landscape of divergence.

Heliconius butterflies have several hybridizing species that provide a powerful system to study the evolution of species barriers. *Heliconius erato* represents an adaptive radiation from Central and South America of about 25 geographic color pattern morphs. These color pattern morphs have evolved to signal their unpalatability to bird predators and mimic locally frequent phenotypes (Mallet and Joron 1999; Chouteau et al. 2016). From within the *H. erato* radiation, two populations are known to show reproductively isolating traits beyond the ecological postmating isolation from selection on warning coloration: *H. himera* from Andean valleys in Ecuador is known to have premating isolation based on mate choice but little or no post-mating reproductive barriers (McMillan et al. 1997; Merrill et al. 2014) and *H. e. chestertonii* occurring in Colombia is known to have both premating isolation based on mate choice and postmating isolation resulting from sex-chromosome linked incompatibilities (Muñoz et al. 2010; Van Belleghem et al. 2018). Despite mate preference between *H. erato* and *H. himera*, they are known to hybridize across at least three geographically distinct contact zones. *Heliconius himera* is found in dry forest areas of southern Ecuador and northern Peru (Jiggins et al. 1996). It comes into contact with *H. e. cyrbia* on the western slopes of the Ecuadorian Andes and with *H. e. favorinus* and *H. e. emma* on the eastern slopes of the Andes, both areas with wet forest (Fig. 1). Hybridization is ongoing and hybrids are easily identifiable by their wing color patterns. In Ecuador, hybrids compose approximately 5% of the population in the contact zone (McMillan et al. 1997), and, although poorly characterized, hybridization is known to occur in the other contact zones.

Here, we focus on reconstructing the history of divergence between the two hybridizing *Heliconius* butterfly species *Heliconius erato* and *Heliconius himera*, and the extent to which isolation and selection have shaped their genomic divergence. First, we start by characterizing the genome-wide divergence patterns among several of the hybridizing *H. erato* populations that vary in their degree of reproductive isolation (*RI*), which we compare to patterns of divergence across three contact zones between *H. erato* and *H. himera*. We use these data to explore the relationship between *RI* and genomic divergence and test whether the *H. erato* x *H. himera* comparisons show the expected patterns of divergence based on the degree of *RI* between the species, when compared to other populations that show weaker or greater degrees of RI. Placing *H. erato* × *H. himera* in the spectrum of RI across the erato clade allows us to better understand the relationship between incomplete barriers and the realized intermediate patterns of genomic divergence. To understand this, we construct demographic models of their evolutionary history from genome-wide SNP data that we use to explore the extent that isolation and selection have shaped genomic divergence. For example, we use coalescent simulations informed by the demographic models to test whether selection can explain the observed heterogeneity of divergence and admixture across the genome. Specifically, the coalescent simulations explore the genome-wide impact of selection on linked sites. Selection on an allele within one population will increase divergence between populations and the amount of genomic sites linked to this pattern will be dependent on the local recombination rate (Kaplan et al. 1989). Hence, we expect a negative association between recombination rate and divergence across the genome (Keinan and Reich 2010; Brandvain et al. 2014; Aeschbacher et al. 2017; Stankowski et al. 2019). This pattern, however, is not indicative of a barrier locus, because such pattern could arise from selective sweeps within populations even between geographically isolated populations. Instead, if the species continue to hybridize and selection acts against introgression at many sites throughout the genome, we may expect a positive association between recombination rate and admixture. This is because neutral alleles in regions with a high recombination rate will be more likely to escape selection at nearby barrier loci and introgress (Barton and Bengtsson 1986; Schumer et al. 2018; Martin et al. 2019). This latter pattern would not be expected if they diverged in isolation (Nachman and Payseur 2012; Aeschbacher et al. 2017). Thus, we can use the relationships of recombination rate with divergence and admixture to infer the relative importance of selection at many loci during speciation.

In contrast to the relatively high rates of current hybridization between the *H. erato* and *H. himera* species pair, which fit well with intermediate levels of both *RI* and genomic divergence, our demographic models suggest that a period of reduced migration rates and subsequent admixture have contributed to the observed heterogeneous patterns of genomic divergence. Moreover, coalescent simulations that explore a scenario of recent and strong selective events on linked sites in the absence of gene flow best fit the observed relationship of genomic divergence, admixture, and recombination rate in *H. erato* and *H. himera*. Despite

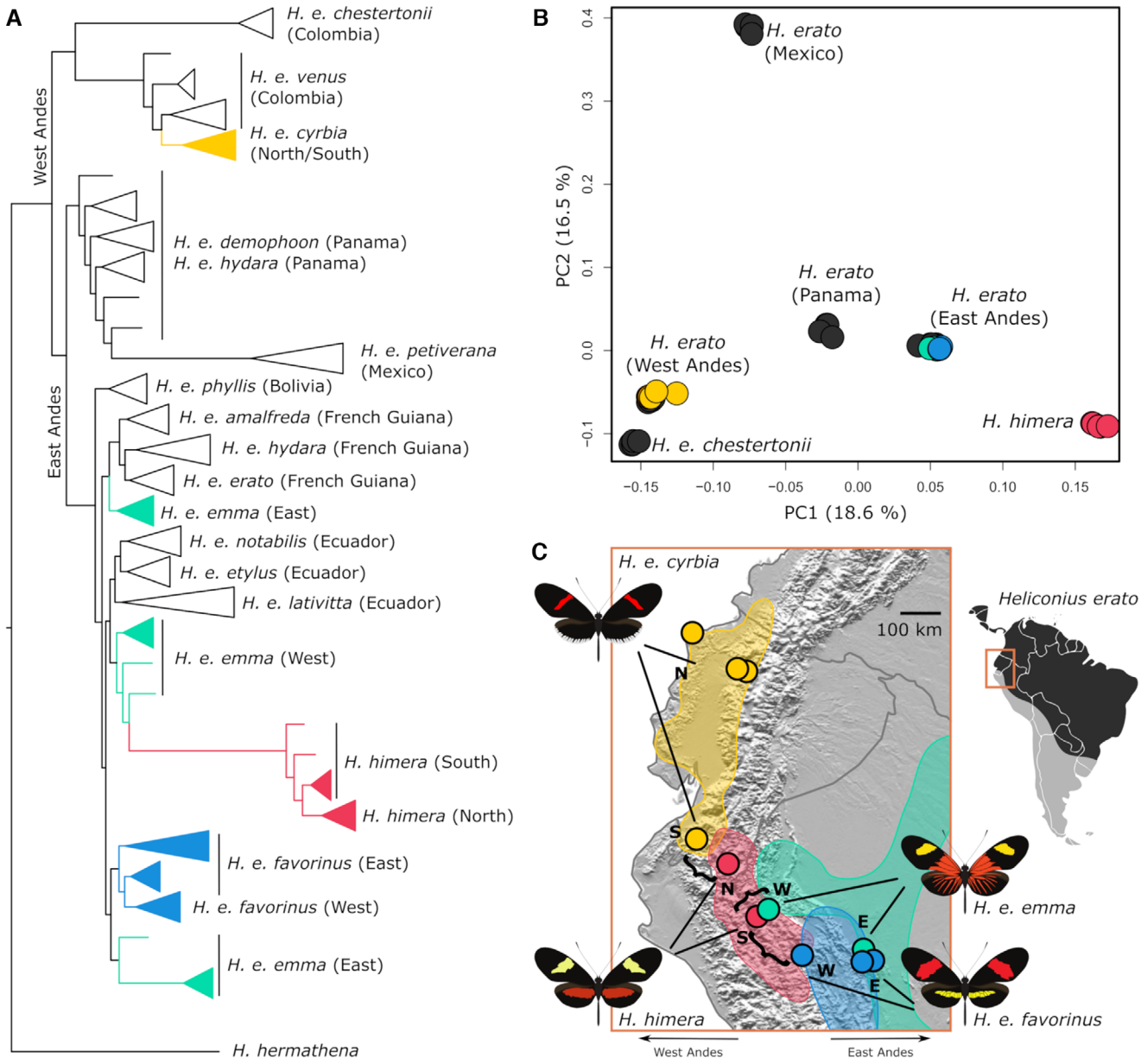

Figure 1. **Geographical distribution, population structure and phylogeny of the focal populations in relation to the *Heliconius erato* radiation. (A) Maximum likelihood tree built using FastTree and using only autosomal sites from 121 whole genome resequenced individuals (see Fig. S1 for the uncollapsed tree). Nodes in the tree that represent the major clades within *H. erato* (east and west of Andes) obtained high support (= 1) from the Shimodaira-Hasegawa test. (B) Principal Component Analysis (PCA) of the focal samples (colored points) among all the available whole genome data for the *H. erato* radiation (black points). (C) We sampled *H. himera*, *H. e. cyrbia*, *H. e. emma* and *H. e. favorinus* from two separate geographic areas each, indicated as North, South, East or West. The distribution of *H. himera* (red) covers dry valleys in the Andes of South Ecuador and North Peru. In the North, *H. himera* (N) comes into contact with a western *H. e. cyrbia* (S) population. In the South, *H. himera* comes into contact with an eastern *H. e. emma* (W) and *H. e. favorinus* (W) population. These contact zones are indicated with parenthesis.**

this history of isolation, we also show that the current species boundary between *H. himera* and *H. erato* is porous and that signals of recent admixture are asymmetrical, suggesting higher gene flow from *H. himera* into *H. erato*. We suggest that this asymmetrical signal of gene flow may be the result of either a polygenic architecture of the species boundaries that restrict introgression into *H. himera* or adaptive introgression of *H. himera* alleles into *H. erato*. Overall, our results highlight the contribution of both isolation and selection to the heterogeneous genomic divergence patterns between the species pair *H. erato* and *H. himera* and help us understand how demographic and selective processes contribute to speciation.

Methods

GENOMIC SAMPLING

We obtained whole genome resequence data for a total of 122 *Heliconius* butterflies with a coverage between 15 to 30× (112 previously published and 10 *H. e. cyrbia* from North Ecuador newly sequenced; Table S1). These include *H. e. cyrbia* to the north (North Ecuador, $n = 10$) and south (South Ecuador *H. himera* contact zone, $n = 4$), *H. e. emma* to the west (Peru *H. himera* contact zone, $n = 4$) and east (Peru *H. e. favorinus* contact zone, $n = 7$) and *H. e. favorinus* to the west (Peru *H. himera* contact zone, $n = 4$) and east (Peru *H. e. emma* contact zone, $n = 8$). We used these populations to study admixture patterns with *H. himera* to the north (Ecuador *H. e. emma/favorinus* contact zone, $n = 5$) and south (Peru *H. e. cyrbia* contact zone, $n = 4$). Additionally, samples from *H. e*. petiverana (Mexico, $n = 5$), *H. e. demophoon* (Panama, $n = 10$), *H. e. hydara* (Panama, $n = 6$ and French Guiana, $n = 5$), *H. e. erato* (French Guiana, $n = 6$), *H. e. amalfreda* (Suriname, $n = 5$), *H. e. notabilis* (Ecuador *Heliconius erato lativitta* contact zone, $n = 5$ and Ecuador *H. e. etylus* contact zone, $n = 5$), *H. e. etylus* (Ecuador, $n = 5$), *H. e. lativitta* (Ecuador, $n = 5$), *H. e. phyllis* (Bolivia, $n = 4$), *H. e. venus* (Colombia, $n = 5$), and *H. e. chestertonii* (Colombia, $n = 7$) were used for contact zone divergence analysis and population structure visualization as well as samples of *H. hermathena* (Brazil, $n = 3$) as an outgroup to root the phylogenetic inference and polarize site frequency spectra. All data have been previously published (Van Belleghem et al. 2017, Van Belleghem et al. 2018), apart from the ten *H. e. cyrbia* from North Ecuador. Genotypes were obtained as in Van Belleghem et al. (2018), see Supporting Information Methods for details.

GENOMIC DIVERGENCE AND PHYLOGENETIC RELATIONSHIPS

We estimated levels of relative divergence (F_{ST}) (Hudson et al. 1992) between populations in non-overlapping 50 kb windows using Python scripts and egglib (De Mita and Siol 2012). For this analysis, we only considered windows for which at least 10% of the positions were genotyped for at least 75% of the individuals within each population. On average 96% of windows met this criterion. To discern population structure among the *H. erato* and individuals, we performed principal component analysis (PCA) using EIGENSTRAT SmartPCA (Price et al. 2006). For this analysis, we only considered autosomal biallelic sites that had coverage in all individuals, were at least 1000 bp apart and excluding the Z chromosome (164,398 SNPs). Using autosomal biallelic sites that had coverage in all individuals and including the outgroup *H. hermathena* (4,927,152 SNPs), we used FastTree version 2.1 (Price et al. 2010) to infer an approximate maximum likelihood phylogeny using the default parameters.

MEASURE OF REPRODUCTIVE ISOLATION

We correlated measures of Reproductive Isolation (*RI*) with patterns of genome-wide divergence between hybridizing pairs of *H. erato* color pattern morphs, *H. himera* and *H. e. chestertonii*. *RI* was estimated for 13 hybridizing pairs from the *H. erato* clade using information on isolating barriers from existing literature and the methods of Sobel and Chen (2014). For each pair, the strength of post-mating barriers due to selection on individual color pattern loci was determined using selection coefficients based on cline widths for the color pattern loci (Mallet 1986, 1993; Mallet et al. 1990; Jiggins et al. 1996; Shaak 2015), premating isolation due to sexual selection was obtained from previous mate preference studies (Jiggins et al. 1996; Muñoz et al. 2010; Merrill et al. 2014), and post-mating isolation estimates due to hybrid inviability that has been reported for *H. e. chestertonii* and *H. e. venus* was obtained from Muñoz et al. (2010). For more details on estimates of each of the Reproductive Isolation (*RI*) values, see Supporting Information Methods. To estimate Total Isolation (*TI*) for each hybridizing pairs, we used the *RI* values for each individual barrier and the *TI* calculator from Sobel and Chen (2014). We have included a version of the Sobel and Chen (2014) *RI* calculator in the supplementary information, to show the values of *RI* for each barrier used to estimate *TI* (Table S2).

DEMOGRAPHIC MODELING

To infer the demographic history of the *H. erato* and *H. himera* populations, we used the joint site-frequency spectra (JSFS) of five population comparisons and a modified version of *∂a∂i* version 1.7 (Gutenkunst et al. 2009). The five population comparisons included the three *H. erato* and *H. himera* hybrid zones plus a comparison of the *H. erato* populations east and west of the Andes and between *H. e. emma* and *H. e. favorinus*. Models tested include four basic scenarios in addition to 22 extensions of the basic models that allowed for independent assessment of additional selective and demographic parameters, including a growth rate parameters (g), heterogeneity in N_e across the genome ($2N$), heterogeneous migration rates ($2m$) (Rougeux et al. 2017; Table S3).

To check for model convergence, a total of 20 independent optimizations were performed for each model on each population comparison. When running these models, consistency in the likelihood scores generally increased as the best optimized parameters from previous steps were incorporated into subsequent steps. To score the models and account for overparameterization, the Akaike Information Criterion (AIC: Burnham and Anderson 2004) was used and parameters from the top five scoring runs for each model were averaged. The models with the best average AIC score were retained for each comparison. The highest and lowest optimized parameter values in the top five replicate runs for each model were used to construct intervals to estimate

uncertainty. For details on SNP filtering, demographic model extensions, and transformation of parameter estimates to absolute units, see Supporting Information Methods.

ADMIXTURE STATISTICS

We estimated admixture proportions for 50 kb non-overlapping windows using the f_d statistic (Martin et al. 2015a). This statistic is based on the ABBA-BABA test or Patterson's *D* statistic that measures an excess of derived allele sharing between sympatric non-sister taxa in a tree of three populations and an outgroup with the relationship (((P1, P2), P3), O) (Durand et al. 2011; for details see Supplemental Methods). The populations included as P1, P2, and P3 are indicated in the figures. *Heliconius hermathena* samples were consistently used as the outgroup taxa (O).

To quantify the distribution of tracks in the genome with high f_d in the hybrid zones, we modeled a loess regression to the f_d data in R (span = 0.005, degrees of freedom = 2). We obtained tracks of multiple adjacent 50 kb windows with high f_d where a loess fit rose above an f_d threshold of 0.062 for the *H. himera – H. e. cyrbia* and *H. himera - H. e. emma* comparisons and above an f_d threshold of 0.071 for *H. himera – H. e. favorinus* comparisons. While these f_d thresholds represent a low absolute proportion of admixture for that window, we note that a single *H. erato* sample carrying an allele with ancestry from *H. himera* would result in an admixture proportion of maximally 0.125 if 4 samples are used in each population for the admixture test. Further, as f_d estimates generally give a substantial underestimate of expected admixture proportions (∼0.5 lower, see Martin et al. 2015a), we used half of the expected admixture proportion for a single individual (0.063) as a threshold for admixture in our loess fit regression. While this is likely an approximation, visual inspection between of the extracted high f_d tracks shows that these generally match well to sharp increases in f_d at multiple adjacent 50 kb windows. To understand whether the f_d tracks result from single introgressed haplotypes rather than from multiple smaller haplotypes introgressed in multiple individuals, we compared the f_d signals to relative divergence patterns between *H. himera* and single individuals of *H. erato*. For this, we used the measure d_a, which subtracts the average nucleotide diversity of both populations from pairwise nucleotide differences (d_{XY}) between populations (Nei and Li 1979). These analyses allowed us to address whether the length of f_d tracks could be explained by introgression of multiple smaller haplotypes from *H. himera* into *H. erato*. If we found that track lengths of low divergence, when using single *H. erato* individuals, corresponded to the tracks of high f_d, this would suggest that the high f_d tracks can be explained by introgression of single long haplotypes from *H. himera* into *H. erato*, rather than resulting from the introgression of several tightly linked haplotypes in multiple individuals.

ADMIXTURE DIRECTIONALITY

By expanding the four-taxon *D* statistic to a five-taxon scenario, it is possible to obtain information on the directionality of admixture (i.e., donor versus recipient population). A set of statistical measures that use a five-taxon symmetric phylogeny to infer both the taxa involved in and the direction of admixture are called the D_{FOIL} statistics (Pease and Hahn 2015; for details see Supporting Information Methods). We assessed admixture directionality in 50 kb non-overlapping windows in the three *H. himera* contact zones with *H. erato* populations using the available *dfoil* software (www.github.com/jbpease/dfoil). Samples from the *H. himera* North and South populations were specified as the P1 and P2 group, whereas samples from the considered *H. erato* populations were specified as P3 and P4. *Heliconius hermathena* was used as the outgroup taxon (ID hermathena_13 in Table S1). The D_{FOIL} statistics were calculated between each possible combination of available ingroup taxa (i.e., one sample for each taxon group); 800 combinations for *H. himera – H. e. cyrbia*, 500 for *H. himera – H. e. emma* and 480 for *H. himera – H. e. favorinus*. Among these sample combinations, significant D_{FOIL} signatures (χ^2 goodness-of-fit test) were counted and used to obtain heterogeneous patterns of admixture directionality along the genome.

RECOMBINATION RATE ESTIMATES

We estimated fine-scale variation in population recombination rate ($\rho = 4N_e r$; r = probability of recombination per generation per bp) along the *H. erato* chromosomes from linkage-disequilibrium in population genetic data using *LDhelmet* version 1.7 (Chan et al. 2012). Individual genotypes were phased from 13 *H. erato* populations (i.e. *H. e. cyrbia*, *H. e. venus*, *H. e. demophoon*, *H. e. hydara* (Panama), *H. e. emma*, *H. e. etylus*, *H. e. lativitta*, *H. e. notabilis*, *H. e. favorinus*, *H. e. phyllis*, *H. e. erato*, *H. e. hydara* (French Guiana), and *H. e. amalfreda*) using Beagle version 4.1 (Browning and Browning 2016) with default parameters. To reduce the potential effect of locus-specific changes in effective population size (N_e) on population recombination rate (ρ) estimates (e.g., due to population specific selective sweeps or background selection), we estimated ρ for each *H. erato* population separately and obtained averages across50 kb interval (see Supplemental Methods for details).

DIVERGENCE AND ADMIXTURE SIMULATIONS

To compare patterns in our data to expectations, we simulated genealogies near a selected locus. Genealogies were simulated using the coalescent simulator *msms* (Ewing and Hermisson 2010) and from these genealogies 10 kb sequences were simulated (For details see Supporting Information Methods). The genealogies were sampled at 100 kb increments from the selected locus. This was achieved by using an infinite recombination sites model and changing the position of the selected locus in increments of 10

neutral locus units (i.e., 10×10 kb) away from the sampled locus. Divergence (F_{ST}) was calculated as in Hudson et al. (1992) and admixture (f_d) was calculated as in Martin et al. (2016) using Python scripts and *egglib* version 3 (De Mita and Siol 2012). We investigated the correlation between F_{ST}, f_d and recombination rate at a distance of 500 kb from a selected locus but similar expectations are obtained from wide range of distances to the selected locus. Simulations were run with 100 replicates for each parameter combination. Pseudocode to run the *msms* command lines are provided in Table S4.

Results

PHYLOGENETIC RELATIONS

As previously observed in Van Belleghem et al. (2017), phylogenetically, two distinct clades can be recognized within the *H. erato* radiation: a clade west of the Andes and a clade east of the Andes (Fig. 1A). The clade west of the Andes also includes populations from Panama and Mexico. The newly obtained sequences of the *H. e. cyrbia* population from North Ecuador are phylogenetically indistinguishable from the South Ecuador populations. *Heliconius himera* and *H. e. chestertonii* form distinct genetic clusters, separated from geographically closely related *H. erato* populations (Fig. 1B). We find increased divergence between *H. himera* and *H. erato* from the western Andes slopes compared to *H. erato* from eastern Andes slopes. As seen in the PCA and phylogenetic inference, this results from a deeper split between *H. himera* and *H. e. cyrbia* from the western Andes slope compared to *H. himera* and the *H. erato* that are found east of the Andes, including *H. e. emma* and *H. e. favorinus* (Fig. 1A, B). This is consistent with previous phylogenetic studies that placed *H. himera* nested within the *H. erato* clade and not as a sister species to *H. erato* (Supple et al. 2015; Van Belleghem et al. 2017).

REPRODUCTIVE ISOLATION AND GENOMIC LANDSCAPES OF DIVERGENCE

Correlations of *RI* with genome-wide estimates of relative divergence (F_{ST}) show that divergently selected color patterns between hybridizing color pattern morphs of *H. erato* are likely not sufficient to drive genome-wide increases in divergence when pre- or post-mating barriers are absent (Fig. 2A). In these hybridizing *H. erato* morphs, there are only narrow peaks of divergence largely centered over the loci known to be responsible for color pattern differences (Fig. 2B). In contrast, genomic divergence was highest and elevated genome-wide between *H. e. venus* and *H. e. chestertonii* from Colombia, where both mate preference and hybrid inviability have been reported (Muñoz et al. 2010). As predicted, the *H. erato* and *H. himera* comparisons showed intermediate levels of divergence that corresponded to their relatively stronger, but incomplete levels of reproductive isolation. Across all three studied contact zones between *H. erato* and *H. himera*, divergence has increased to the extent that F_{ST} peaks near the known color pattern loci *WntA* (chr 10), *cortex* (chr 15), and *optix* (chr 18) are largely not detectable (Fig. 2B). However, there are clear differences in the degree of divergence between the species among the three contact zones, with the *H. himera* and *H. erato* contact zones on the eastern Andes (*H. e. emma* and *H. e. favorinus*) showing lower overall genomic divergence than in the western Andes contact zone. Also as expected, we observe a notable increase in divergence on the Z chromosome relative to the autosomes (Fig. 2) that appears to be accentuated with stronger reproductive isolation. This is in line with previous work on *H. e. chestertonii*, which suggested Z chromosome divergence was inflated by an important barrier to gene flow (Van Belleghem et al. 2018).

DEMOGRAPHIC MODELING

We compared the estimated joint site-frequency spectrum (JSFS) for the three geographically distinct contact zones between *H. erato* and *H. himera* to 26 alternative demographic scenarios that varied in split times, migration rates and population sizes. All three *H. erato* and *H. himera* contact zones best fit models that included secondary contact (SC) after a period of isolation without gene flow (Figs. S2 and S3; Table S5). Figure 3 presents a composite of the best model for each pairwise *H. erato* and *H. himera* hybrid zone comparison plus a comparison of the *H. erato* populations east and west of the Andes and between *H. e. emma* and *H. e. favorinus* (parameter estimates of best pairwise $\partial a \partial i$ models is shown on Table S6). We also performed demographic modeling using geographic population subsets as a check to make sure that additional geographic population structure does not change our main results (Table S5). For all three zones we found support for asymmetrical migration. In each case, migration rates were predominantly in one direction, with on average 0.5 to 0.6 migrants per generation moving from *H. erato* into *H. himera*, compared to 0.07 to 0.13 moving from *H. himera* into *H. erato*. This result would be consistent with the effective migration rates being driven by the marked population size differences between the two species (Fig. 3B).

Nearly all the models that included exponential population growth (G) best fit the JSFS, with the exception of the *H. himera* and *H. e. emma* comparison. Estimates of ancestral and contemporary population sizes suggest strong expansions in *H. himera* and *H. erato*. These inferred changes in population sizes broadly fit previous results obtained from pairwise sequentially Markovian coalescent (PSMC) analysis (Van Belleghem et al. 2018), which suggested an overall population growth in *H. erato* east and west of the Andes in the past 1 million years ago and size reduction for *H. himera* in the past 200,000 years ago (Fig. S4).

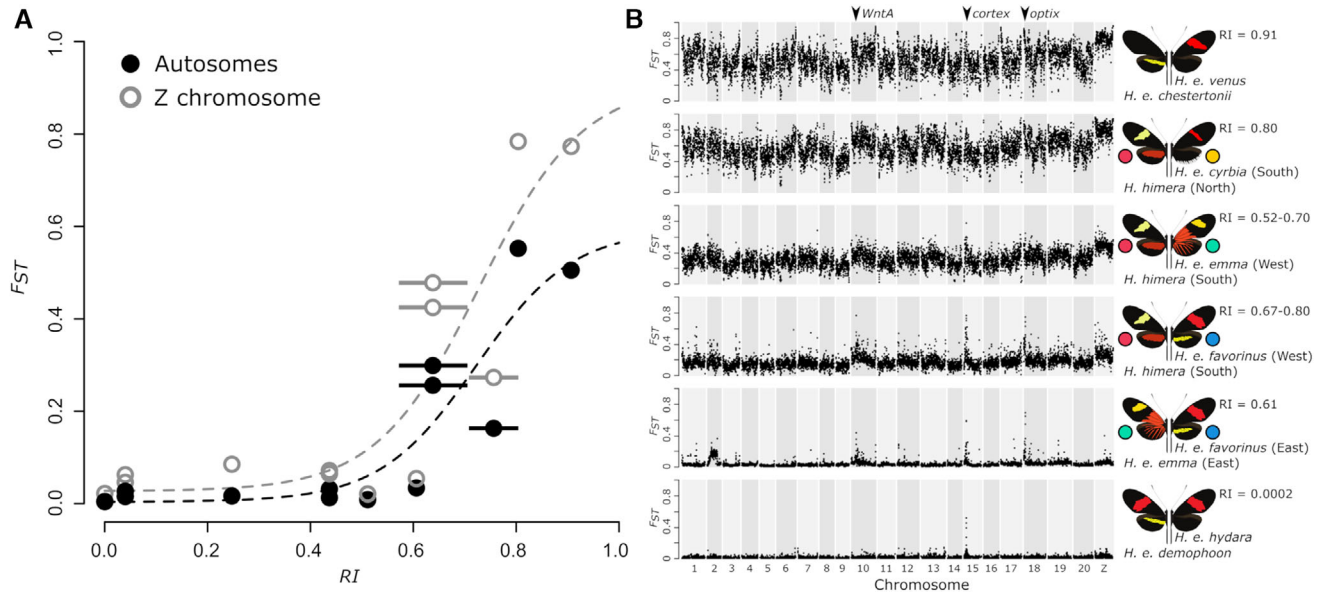

Figure 2. **Reproductive isolation and divergence among *Heliconius erato* populations. (A) Genome-wide averages of relative divergence (F_{ST}) show a sharp increase with increasing measures of reproductive isolation between parapatric *H. erato* populations. The measure of reproductive isolation (*RI*) was obtained by weighting ecological (RI_{ec}), pre-isolation (RI_{pre}) and post-isolation (RI_{post}) components using the method of Sobel and Chen (2014) (Table S2). Horizontal bars indicate a range of *RI* estimates based on uncertainties in *RI* components. Dashed lines indicate a non-linear least-squares fit for autosome (black) and Z chromosome (gray) relation between F_{ST} and *RI*. Higher relative divergence on the Z chromosome can be observed for the more divergent parapatric comparisons, however, incompatibilities that are potentially Z-linked have only been suggested for *H. e. chestertonii* crosses (Muñoz et al. 2010; Van Belleghem et al. 2018). (B) Plots of relative divergence (average F_{ST} in 50 kb windows) between parapatric *H. erato* populations along the genome. Plots are ordered according to the measure of reproductive isolation (*RI*). Colored circles match color codes used for the focal populations in this study. Divergence peaks on chromosome 10, 15 and 18 correspond to the divergently selected color pattern genes *WntA* (affecting forewing band shape), *cortex* (affecting yellow hindwing bar), and *optix* (affecting red color pattern elements), respectively (Van Belleghem et al. 2017).**

However, we found that estimates of contemporary population sizes varied greatly depending on the population comparison (Fig. 3B, C), a result possibly explained by unaccounted population structure and difficulties in estimating growth (G). For *H. e. favorinus*, estimates of contemporary population size were generally much smaller than the ancestral population. This result fits the observation that *H. e. favorinus* is a smaller Andean population of the "postman" color pattern (i.e., red forewing band). Collectively, the models support a history that includes periods of allopatry, followed by lineage specific changes in population size that coincide with more recent gene flow.

To investigate if the JSFS contained evidence of selection driving patterns of divergence across the contact zones, we incorporated heterogeneity in population size (2N) and migration rate (2M) into the models, similar to Rougeux et al. (2017) and Tine et al. (2014), respectively. The 2N model allows heterogeneity in population size estimates across loci that result from the differences in allelic variation caused by linked selection (*ls* = effective population size of locus relative to neutral loci; Q = proportion of the genome affected by *ls*). We found that all contact zones between *H. erato* and *H. himera* well supported 2N models, suggesting the effect of linked selection in shaping patterns of genomic variation and divergence between the species. The strongest *ls* was observed for the population comparisons of *H. erato* East and West ($ls = 0.10$; $Q = 0.35$) and *H. himera* and *H. erato* West ($ls = 0.15$; $Q = 0.90$) and the lowest observed between *H. e. emma* and *H. e. favorinus* ($ls = 0.07$; $Q = 0.04$; Fig. 3C; Table S6).

Selection on locally adapted alleles will also result in regions containing these variants showing much lower rates of migration compared to the rest of the genome. The 2M models allow for this type of heterogeneity in migration rates across the genome. Both contact zones in the eastern Andes supported these models for *H. himera* and *H. erato*, suggesting that these populations have genomic regions with much lower rates of introgression than other parts of the genome.

ADMIXTURE DIRECTIONALITY

To investigate the impact of hybridization on genomic divergence, we explored patterns of admixture along chromosomes for

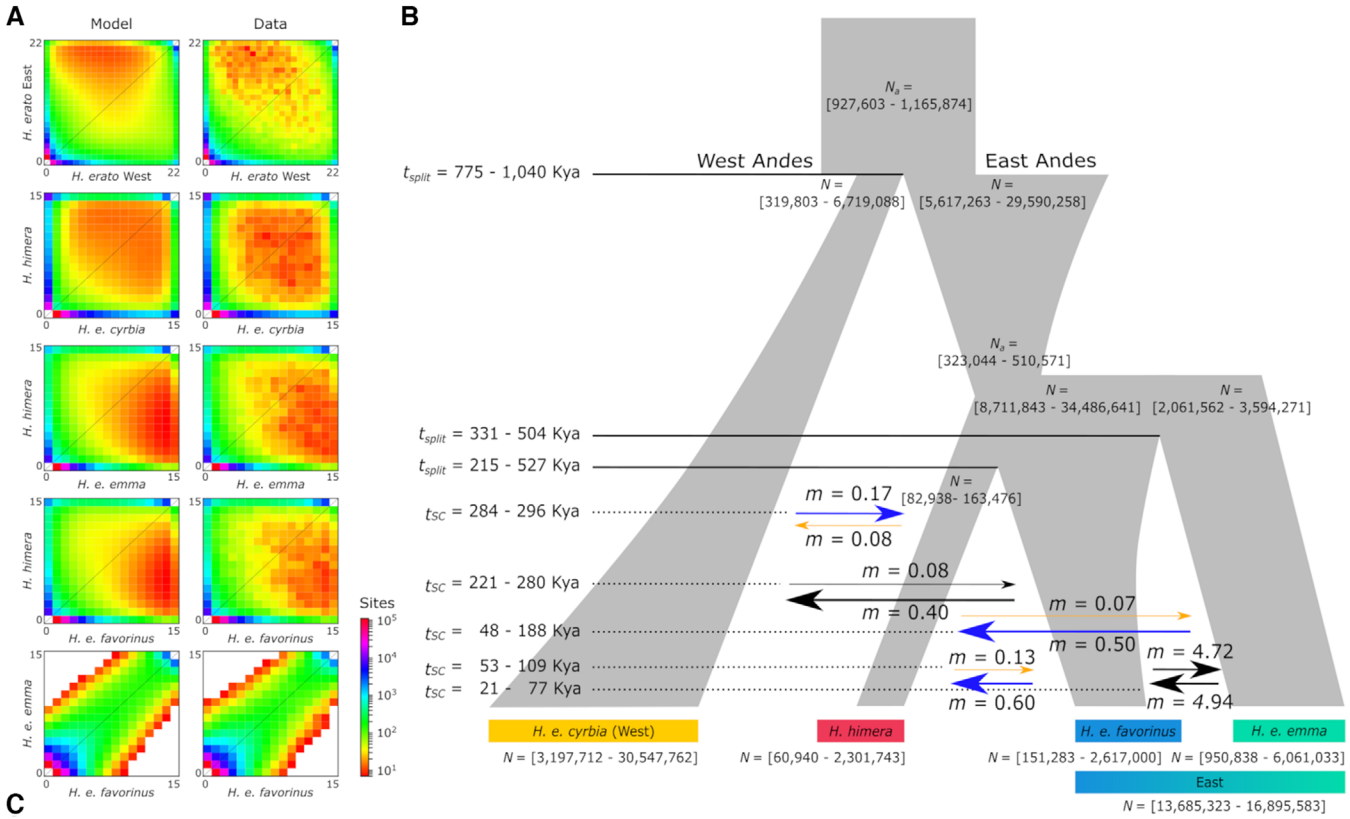

C

Comparison	Best Model	t_{split} (years)	t_{SC} (years)	$m_{1<-2}$	$m_{2<-1}$	$me_{1<-2}$	$me_{2<-1}$	P	ls	Q
H. erato East vs. West Andes	SC2NG	[889531 - 1039826]	[221048 - 279532]	[0.081 - 0.084]	[0.396 - 0.407]	-	-	-	[0.090 - 0.100]	[0.340 - 0.350]
H. himera vs. *H. e. cyrbia*	SC2NG	[774568 - 824039]	[284457 - 296405]	[0.160 - 0.170]	[0.075 - 0.077]	-	-	-	[0.140 - 0.160]	[0.860 - 0.900]
H. himera vs. *H. e. emma*	SC2N2m	[215208 - 527389]	[48373 - 187901]	[0.400 - 0.580]	[0.060 - 0.080]	[0.69 - 1.76]	[0.270 - 4.220]	[0.360 - 0.670]	[0.260 - 2.360]	[0.190 - 0.900]
H. himera vs. *H. e. favorinus*	SC2N2mG	[224160 - 337996]	[53421 - 108780]	[0.500 - 0.690]	[0.100 - 0.160]	[0.58 - 0.98]	[3.960 - 8.320]	[0.510 - 0.620]	[0.180 - 1.580]	[0.070 - 0.870]
H. e emma vs *H. e. favorinus*	SC2N2mG	[331076 - 504316]	[29944 - 112173]	[1.840 - 7.600]	[0.970 - 8.900]	[0.00 - 2.92]	[0.010 - 14.91]	[0.000 - 0.870]	[0.050 - 0.090]	[0.030 - 0.040]

Comparison	Best Model	N_a	N1 [at split]	N2 [at split]	g1	g2	N1 [at sampling]	N2 [at sampling]
H. erato East vs. West Andes	SC2NG	[927603 - 941642]	[26341817 - 29590258]	[319803 - 406187]	[0.520 - 0.570]	[9.990 - 12.74]	[13685323 - 16895583]	[3197712 - 5176219]
H. himera vs. *H. e. cyrbia*	SC2NG	[1146766 - 1165874]	[5617263 - 7292527]	[5669976 - 6719088]	[0.280 - 0.320]	[4.360 - 4.540]	[1554981 - 2301743]	[24746873 - 30547762]
H. himera vs. *H. e. emma*	SC2N2m	[421200 - 482382]	[82938 - 197144]	[2484021 - 5543987]	-	-	-	-
H. himera vs. *H. e. favorinus*	SC2N2mG	[323044 - 348395]	[102651 - 163476]	[8711843 - 34486641]	[0.590 - 0.800]	[0.020 - 0.080]	[60940 - 130182]	[151283 - 2617000]
H. e emma vs *H. e. favorinus*	SC2N2mG	[498501 - 510571]	[2061562 - 3594271]	[17935128 - 25379445]	[0.460 - 1.690]	[0.010 - 0.050]	[950838 - 6061033]	[224427 - 1167647]

Figure 3. **Composite of best pairwise Secondary Contact (SC) demographic models of the *H. himera* and *H. erato* population history using ∂a∂i. (A) Joint Site Frequency Spectra (JSFS) for data and best model (see Table S5 and Figure S2-3 for AIC values (Akaike Information Criterion)). (B) Reconstruction of historical demography of *H. himera* and *H. erato* populations using models with best AIC scores. All best models included a period of isolation and secondary contact. Arrows indicate effective migration rates ($2N_am$). Migration from *H. himera* into *H. erato* is indicated in orange, migration from *H. erato* into *H. himera* is indicated in blue. (C) Table with parameter ranges obtained from five best scoring models out of twenty runs. N_a = ancestral population size, N_1 = Size of population 1, N_2 = size of population 2, $g1$ = growth coefficient of population 1, $g2$ = growth coefficient of population 2, *ls* = linked selection, Q = proportion of the genome with a reduced effective size due to linked selection (*ls*), $m_{1\leftarrow2}$ = migration from population 2 into 1, $m_{2\leftarrow1}$ = migration from populations 1 into 2, t_{split} = split time, t_{SC} = time of secondary contact, P = proportion of the genome evolving neutrally.**

the three contact zones between *H. erato* and *H. himera*. We were interested in both the patterns of admixture across our three replicate hybrid zones and inferring the direction of admixture. To determine if patterns of admixture were similar across the three contact zones, we used the f_d statistic which indicates admixture proportions (proportion of sites that are shared between taxa) within genomic windows (Martin et al. 2015a). Across several chromosomes we observed long tracks of increased f_d, particularly in the hybrid zone between *H. himera* and *H. e. cyrbia* west of the Andes (Fig. 4A). These high f_d tracks included a total of 37.97 Mb and had an average length of 2.53 Mb (SD = 3.31 Mb) (Fig. S5). High f_d tracks included 35.67 Mb between *H. himera* and *H. e. emma* (average length: 1.00 Mb ± 1.34 Mb) and 29.49 Mb between *H. himera* and *H. e. favorinus* (average length: 1.23 Mb ± 1.017 Mb) and were distributed more evenly along the chromosomes (Fig. 4A). In general, there was a lack of overlap between genomic regions with high f_d in the different hybrid zone comparisons. We found 4.48 Mb (6.5 %) of high f_d tracks were

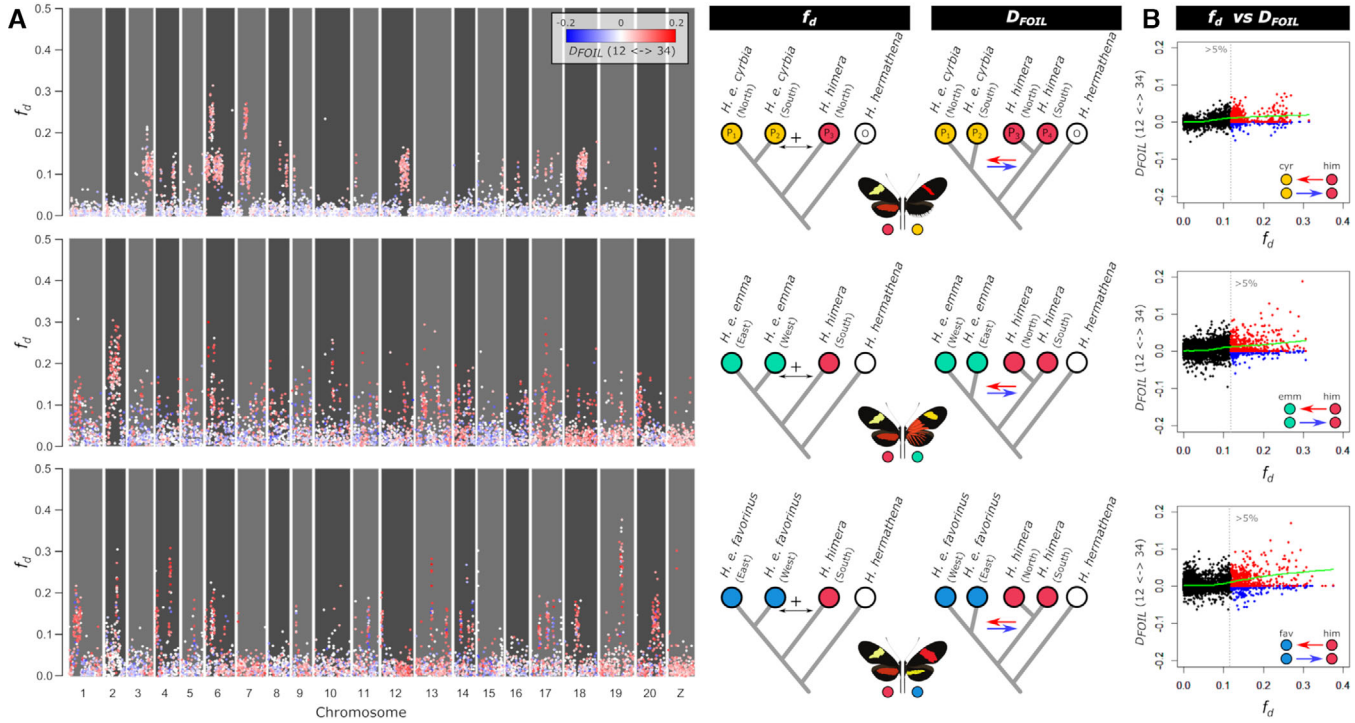

Figure 4. Admixture (f_d) and admixture directionality (D_{FOIL}) between *H. himera* and *H. erato* in three contact zones. (A) Points show admixture (f_d) values, whereas coloring shows directionality (D_{FOIL}) in 50 kb non-overlapping windows for the contact zones *H. himera – H. e. cyrbia* (top), *H. himera – H. e. emma* (middle) and *H. himera – H. e. favorinus* (bottom). Blue indicates predominant admixture from *H. erato* into *H. himera* (12 → 34), whereas red indicates predominant admixture from *H. himera* into *H. erato* (12 ← 34) based on the D_{FOIL} tests. (B) Summary of admixture versus directionality with points above the 95% quantile indicated in blue (12 → 34) and red (12 ← 34) demonstrates that the majority of windows with high f_d indicate admixture from *H. himera* into *H. erato*. The green line indicates a loess fit of the data. Colored circles match color codes in Figure 1.

shared between the *H. himera*/*H. e. cyrbia* and *H. himera*/*H. e. emma* hybrid zone, 3.83 Mb (6.0 %) were shared between the *H. himera*/*H. e. cyrbia* and *H. himera*/*H. e. favorinus* hybrid zone and 8.04 Mb (14.1 %) were shared between the *H. himera*/*H. e. emma* and *H. himera*/*H. e. favorinus* hybrid zone.

To determine the directionality of introgression across the genome we used a five-taxon D_{FOIL}-statistic (Pease and Hahn 2015). This test considers all available taxa (i.e., two populations of *H. himera* and two populations of *H. erato*) and calculates all possible four-taxon *D*-statistic comparisons to infer admixture as well as directionality of admixture. While the D_{FOIL}-statistic is calculated using a single genome for each taxon, we performed this test on all possible combinations of available samples and represented the D_{FOIL} signal as the proportion of significant comparisons (Fig. 4A). Comparing f_d and D_{FOIL} results revealed that among loci that show strong evidence of admixture (high f_d), there is a relative paucity of loci in *H. himera* individuals carrying *H. erato* alleles (Fig. 4B). This result contrasts with the demographic modeling which suggested higher rates of gene flow from *H. erato* into *H. himera* (Fig. 3) and likely results from differences in temporal dynamics measured by each method, with $\partial a \partial i$ models fitting older signals of admixture that are potentially driven by a higher effective population size *of H. erato* compared to *H. himera*. This asymmetry suggests *H. erato* is more porous to introgressed alleles from *H. himera* than vice-versa. Consistent with a well characterized "large X(Z) effect" in speciation, on the sex (Z) chromosome there are only a few loci that show signals of admixture (high f_d) and again the D_{FOIL} tests only show signals of introgression of *H. himera* alleles into *H. erato* on the Z chromosome (Fig. 4A).

Because long tracks of increased f_d may result from either introgression of long haplotypes or introgression at multiple tightly linked loci, we next investigated divergence signals between single *H. erato* individuals from hybrid zones with the *H. himera* populations (Fig. S6). In all three contact zones, we find that many of the high f_d tracks correspond to tracks of reduced divergence between a single *H. erato* individual and *H. himera*. This is in line with the high f_d tracks being largely driven by *H. erato* individuals carrying a haplotype with *H. himera* ancestry.

ASSOCIATION OF DIVERGENCE AND ADMIXTURE WITH RECOMBINATION RATE

Because the effect of selection on linked sites will depend on recombination rate, differences in the relationships between recombination rate and relative divergence (F_{ST}) and between recombination rate and admixture (f_d) can be used to determine how selection may have shaped genomic divergence between *H. erato* and *H. himera*. We first explored this relationship of recombination rate, relative divergence, and admixture across the *optix* locus. The *optix* locus controls red wing pattern differences among *H. erato* color pattern morphs, as well as between *H. erato* and *H. himera* and is a target of strong selection (Fig. 5A) (Counterman et al. 2010; Supple et al. 2015; Van Belleghem et al. 2017). We found recombination rate (ρ) estimates were markedly lower upstream, compared to downstream of the *optix* gene (Fig. 5C). Such sharp decreases in recombination rate near chromosome ends have been observed in other *Heliconius* species (Martin et al. 2019) and likely explain the decrease in recombination rate upstream of the *optix* gene. To test if selection at the *optix* locus has produced the expected negative relationship of recombination rate with divergence and positive relationship of recombination rate and admixture, we visualized these relationships 500 kb from the center of the peak of the divergence at *optix* (Fig. 5D) so they could be directly compared to the simulation results, which were also sampled 500 kb from the target of selection (see "Divergence and admixture simulations"). As expected, we observe a negative relationship between recombination rate and divergence (F_{ST}) but no obvious correlation between recombination rate and admixture (f_d).

To understand how recombination rate variation, selection and admixture have contributed to patterns of genome-wide divergence, we next compared recombination rates with divergence and admixture across the whole genome. In line with expected patterns of linked selection, we found a significant negative association between recombination rate (ρ) and relative divergence (F_{ST}) between *H. himera* and *H. erato* populations (Fig. 5A) but no association with admixture (f_d) (Fig. 6B).We also observed a positive association between the proportion of coding sequence and relative divergence, further suggesting the importance of linked selection for genome divergence (Fig. S7). Additionally, we found a significant negative relationship between F_{ST} and f_d in the *H. himera – H. e. cyrbia and H. e. emma* hybrid zones, which indicates that admixture can partly explain reduced F_{ST} (Fig. 6C).

DIVERGENCE AND ADMIXTURE SIMULATIONS

We used a range of estimates of divergence times, population size changes, and migration from the demographic models to seed coalescent simulations and investigate expected patterns of recombination rate on divergence and admixture rates. Specifically, the simulations test the prediction whether selection (i.e., recent selective sweeps) and isolation (i.e., secondary contact) in the past million year of divergence between *H. himera* and *H. erato* can explain the observed relationships of recombination rate with relative divergence (F_{ST}) and admixture (f_d).

From our demographic models, the split between *H. himera* and *H. erato* (East) was estimated between 215 and 527 thousand years ago. In our simulations this time point fits the split between (P1, P2) and P3, which we modeled at 2 million generations (t_2; Fig. 7A). Assuming a generation time of 0.25 years, 2 million generations match a split of 500,000 years ago. After these populations split, migration (m) was restricted between P2 and P3 only, with symmetrical migration rates starting at time t_m. In accordance with our demographic modeling results, we ran simulations by also varying the parameters t_s (selection start time), m (migration rate) and ρ (population recombination). In Figure 7, we highlight two extreme scenarios of migration and selection start time which we denoted as "Isolation with Migration" (IM) and "Secondary Contact" (IM). As demonstrated by other studies, in a scenario of IM with long periods of migration and divergent selection, our simulations predicted a strong negative correlation between recombination rate and F_{ST} (Keinan and Reich 2010; Brandvain et al. 2014; Crawford et al. 2015) and a strong positive correlation between recombination rate and f_d (Aeschbacher et al. 2017; Martin et al. 2019; Fig. 7C, left). The correlation pattern between recombination rate and F_{ST} reflects the degree of linkage disequilibrium between neutral sites and loci under divergent selection (Charlesworth 1998; Nachman and Payseur 2012). In contrast, our simulations show that the relationship between recombination rate and f_d is reduced when migration is more recent or low (Fig. 7C, left). For example, in a SC scenario that is characterized by a more recent onset of migration, the simulations show that F_{ST} values are generally high and f_d values close to zero (Fig. 7C, right). This results in the absence of a relationship between recombination rate and F_{ST} or f_d in most SC scenarios when the onset of migration started less than 10,000 generations ago and in IM models with migration rates ($2N_em$) lower than 2. However, when selection in the genome is recent (~selective sweeps), a negative relationship between recombination rate and divergence, but not admixture, emerges in the SC scenario (Fig. 7C). This relationship arises due to linked selection that reduces diversity within populations and increases the relative divergence, F_{ST}, between populations over larger genomic regions with lower recombination rate (Cruickshank and Hahn 2014). The relationship holds for lower selection strengths at relatively short distances from the selected site (s = 0.02; Fig. S8).

The simulated secondary contact model is an extreme scenario with recent onset of strong migration (start migration << 100,000 generations). However, similar relationships between

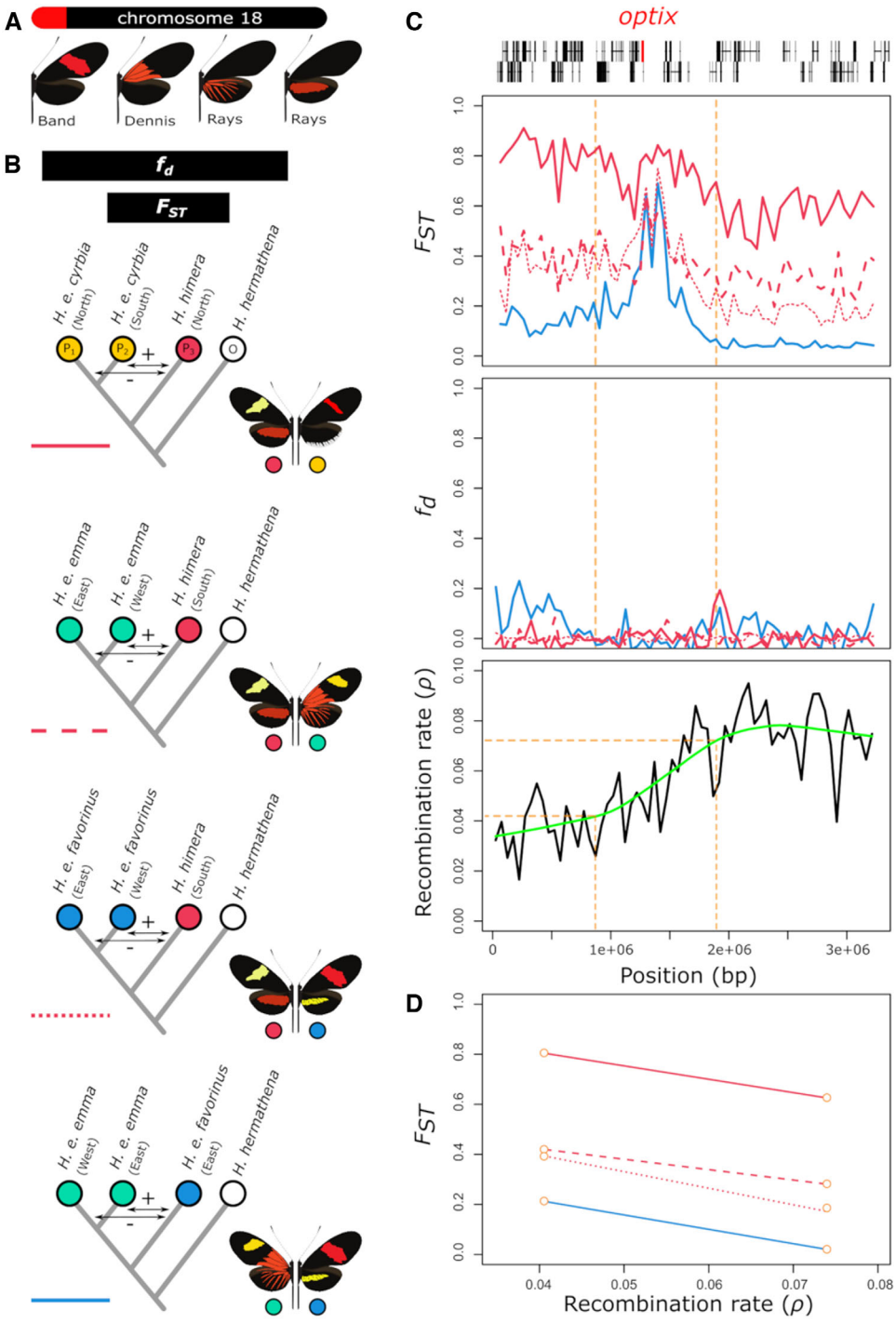

Figure 5. Divergence (F_{ST}), admixture (f_d) and recombination rate (ρ) near the red color pattern gene *optix*. (A) The *optix* gene is located near the start of chromosome 18 and has been demonstrated to control the expression of red color pattern elements in *Heliconius* wings (Reed et al. 2011). (B) Relative divergence (F_{ST}) and admixture (f_d) comparisons performed between *H. himera*, *H. e. cyrbia*, *H. e. emma* and *H. e. favorinus*. Colored circles match color codes in Figure 2. (C) Lines show F_{ST}, f_d and recombination rate (ρ) calculated in 50 kb non-overlapping windows. The green line in the bottom plot shows a loess fit of the recombination rate. Gene models including the location of the *optix* gene are presented at the top. (D) Relationship between F_{ST} and recombination rate (ρ) 500 kb left and right from the center of the *optix* regulatory sequence divergence peak. The relation between f_d *and* recombination rate (ρ) is near zero and not shown.

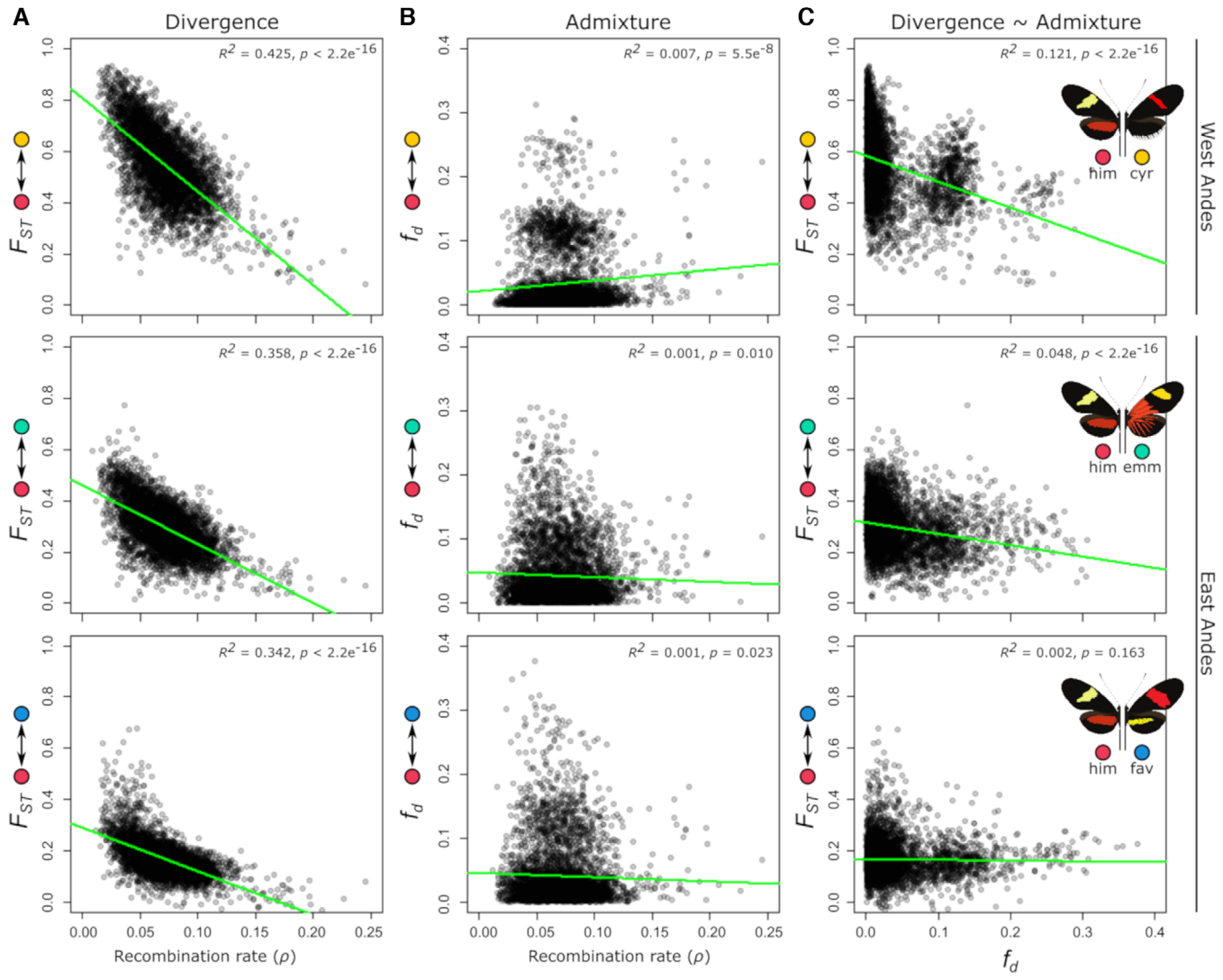

Figure 6. **Correlations of divergence and admixture proportions with recombination rate in the three *H. himera – H. erato* contact zones. (A) Relative divergence (F_{ST}) versus population recombination rate (ρ). (B) Admixture proportion (f_d) versus population recombination rate (ρ). (C) Relative divergence (F_{ST}) versus admixture proportion (f_d). Statistics were calculated in 50 kb non-overlapping windows. Recombination rates were calculated from each *H. erato* population separately and averaged over populations (see methods) and showed a genome-wide average of ρ equal to 0.071 (SD = 0.026; $\rho = 4N_e r$). Colored circles match geographic distributions and contact zones in Figure 2.**

recombination rate, relative divergence and admixture arise in a scenario where secondary contact is older (>> 100,000 generations) but migration rates are low (Fig. 7C). This latter scenario fits the observed demographic estimates for *H. erato* and *H. himera*, with low migration rates ($2N_em < 0.2$) estimated to start at 100,000 - 750,000 generations ago.

Finally, we note that the observed relationship between recombination rate and divergence may include the effects of genetic hitchhiking, selection against gene flow as well as background selection. While our genomic dataset does not allow us to differentiate background selection from genetic hitchhiking and selection against gene flow, our simulations suggest that the observed patterns can be explained by these latter two processes, and other studies suggest background selection may be too subtle to cause these patterns (Stankowski et al. 2019).

Discussion

By relating patterns of genomic divergence to ecological and other barriers to gene flow, our results provide a view into the genomic landscape among lineages with increasing degrees of reproductive isolation (Kronforst et al. 2013; Roux et al. 2016). In line with theoretical expectations of the speciation process (Barton and De Cara 2009; Nosil et al. 2017), the increase in

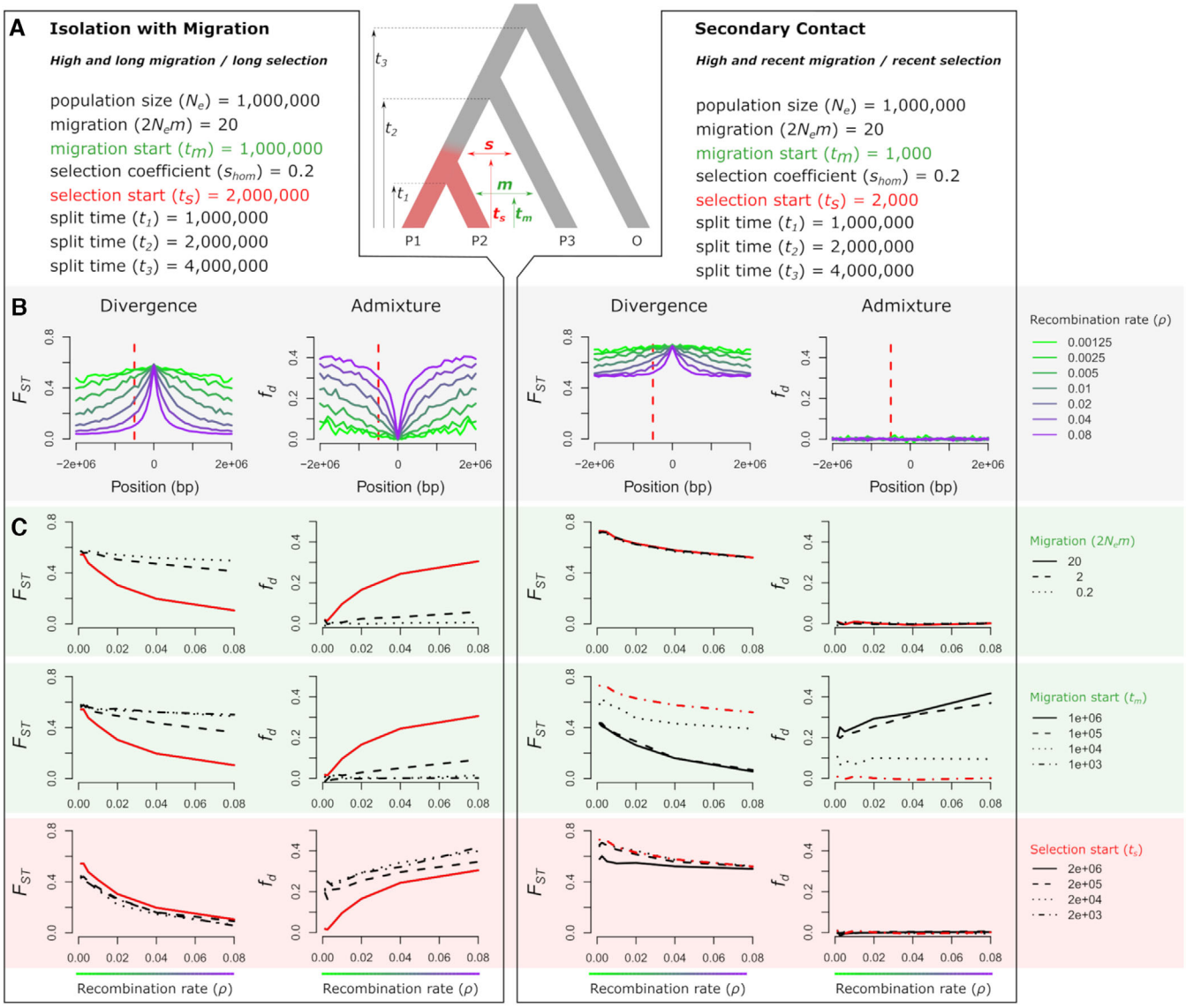

Figure 7. Expected relationship of recombination rate with divergence (F_{ST}) and admixture (f_d) near a divergently selected locus. (A) The population tree shows the simulated scenario with the onset of divergent selection on a derived allele indicated in red and in which migration rate (m) and migration time (t_m) between P2 and P3 and selection start time (t_s) are varied. Left and right of the simulated scenario are parameter combinations for two extreme scenarios that both include linked selection; on the left a scenario with Isolation with Migration (IM) and on the right a scenario reflecting Secondary Contact (SC). (B) Effect of population recombination rate (ρ) on relative divergence (F_{ST}) and admixture (f_d) near a divergently selected locus for the two simulated scenarios with parameter combinations as in panel A. The selected allele occurs at position 0. The dashed red line indicates a locus at 500 kb from the selected locus at which the relationship between ρ, divergence and admixture is assessed in panel C. (C) The effect of migration start time (t_m) and selection start time (t_s) on the relation between ρ, divergence and admixture. Apart from the respective parameters being evaluated, other parameters were fixed as in panel A, with the red lines indicating the exact parameter combinations as in panel A and B. For simulations with a lower selection coefficient (s = 0.02), see Figure S8.

divergence does not seem to be a linear process. Rather, there is a marked increase in divergence associated with assortative mating which has evolved between *H. himera* and *H. erato*, highlighting the global impacts that incomplete pre-mating barriers could have in the genome. We also observed a notable increase in divergence on the Z chromosome relative to the autosomes which supports a large effect of the Z chromosome in the genomic divergence during the early stages of speciation (Sperling 1994; Prowell 1998). Despite being able to reconstruct this progression of genomic divergence from increased reproductive isolation, it remains

difficult to determine if genomic peaks of divergence result from barrier loci that are resistant to ongoing gene flow (heterogeneous gene flow), from recent selective sweeps in isolated populations (heterogeneous selection), or both. Nevertheless, from comparing the observed patterns of genomic divergence with demographic models and coalescent simulations, we can test various hypotheses of the architecture of the species boundaries between *H. erato* and *H. himera* that allow us to determine the extent isolation and selection contribute to the heterogeneous landscapes of divergence.

ARCHITECTURE OF THE SPECIES BOUNDARIES

Our data favors a history of isolation accompanied with selection. From our coalescent simulations, we found that heterogeneity in levels of divergence (F_{ST}) may largely be explained by selection acting on alleles within isolated populations and is not representative of selection against gene flow. In contrast, observed signals of admixture (f_d) and the length of high admixture tracks may reflect a snapshot from recent hybridization events. Although we note that the expectations of admixture track lengths may differ when there is selection against recombinants, we argue that the long length of high f_d tracks compared to the linkage disequilibrium breakdown within 1 to 2 kb estimated in *H. melpomene* (Martin et al. 2016) together with single *H. erato* individuals harboring long haplotypes of *H. himera* ancestry (Fig. S6) suggests these patterns may represent recent and independent admixture events at the three contact zones. The heterogeneous signal of admixture may thus be the result of a few generations of backcrossing of hybrid individuals even in the absence of selection. Nevertheless, whether introgressed haplotypes may become purged by selection or result from adaptive introgression is hard to predict with the current data. One possibility is that the multitude of loci with asymmetrical gene flow from *H. himera* into *H. erato* represents the genetic signal of a polygenic species barrier. These barriers could result from co-adapted loci in *H. himera* that cannot be replaced by *H. erato* alleles without fitness consequences. The inference that this pattern of asymmetrical gene flow results from a polygenic species barrier and not from mate choice directionality or demographic factors (e.g., larger effective population size of *H. erato*) is further strengthened by two observations. First, *H. himera* males have been shown to mate more frequently with F1 hybrids compared to *H. erato* males (McMillan et al. 1997), which should result in an opposite asymmetric admixture pattern than what we found (Latour et al. 2013), with more alleles introgressing from *H. erato* into *H. himera*. Second, the smaller effective population size estimates of *H. himera* should also result in the same opposite pattern of asymmetric admixture (Frantz et al. 2014). This latter expectation is observed in the demographic modeling results, which show greater migration of alleles from *H. erato* into *H. himera* and corresponds to their estimated differences in population size between the species (Fig. 3B) but is not seen in the more recent signals of admixture as measured by f_d. This discrepancy between the migration rates estimated from the demographic modeling and the f_d statistic potentially results from differences in the temporal dynamics measured by each method, with $\partial a \partial i$ models fitting older signals of admixture.

The finding that selection at multiple loci may have resulted in a polygenic species boundary would add to a number of studies that illustrate how pervasive selection along the genome can lead to the evolution of polygenic architectures of species boundaries (Brandvain et al. 2014; Janousek et al. 2015; Aeschbacher et al. 2017; Berner and Roesti 2017; Martin et al. 2019). This is also consistent with evidence that many loci contribute to population divergence among hybridizing population in the *H. erato* clade (Lewis et al. 2020). However, it also possible that asymmetrical adaptive introgression could contribute to the observed patterns of divergence and admixture between *H. erato* and *H. himera*. Adaptive introgression has been well documented at color pattern loci across *Heliconius* (Dasmahapatra et al. 2012; Wallbank et al. 2016; Van Belleghem et al. 2017; Edelman et al. 2019) but larger genomic datasets are often needed to perform these more rigorous tests for signatures of selection and introgression (Edelman et al. 2019; Meier et al. 2020; Moest et al. 2020). We find very few genomic regions that show admixture across all three *H. himera* and *H. erato* contact zones, which would be expected if these regions represent random tracts of admixture from recent gene flow, but not if adaptive introgression were driving admixture of specific alleles with selective advantage. Therefore, it seems possible that the patterns reflect a polygenic species boundary driven by selection against gene flow. However, further data and analyses are needed to assess the possible contribution of adaptive introgression.

DIFFERENT HISTORIES CAN GENERATE SIMILAR HETEROGENEOUS DIVERGENCE PATTERNS

Although the genomic landscape of divergence between hybridizing taxa reflects the history of selection and demographic changes they have experienced, different histories can generate strikingly similar heterogeneous patterns. This can greatly limit our ability to make inferences about the evolutionary processes driving genomic change (Ravinet et al. 2017). For example, in *Heliconius melpomene* there is, at first sight, a similar heterogeneous landscape of divergence to those we report here for *H. erato* and *H. himera*, despite known differences in their evolutionary histories (Quek et al. 2010; Martin et al. 2013). *Heliconius melpomene* and *H. erato* are co-mimics and experience similar strong selective pressures on wing color patterns throughout their distributions. In the *H. melpomene* clade, *H. melpomene* comes into contact and hybridizes with *H. cydno* in Panama and occasionally with *H. timareta* in Ecuador and northern Peru. Although the

genomic landscapes in the erato and melpomene clades appear similar at first sight, correlation analyses reveal potential differences in the relative importance of admixture. The *H. melpomene* comparisons showed strong correlations of recombination rate with divergence as well as admixture, which supports a long history of divergent selection with gene flow (Martin et al. 2019) and agrees with our coalescent simulations. In contrast, *H. himera* and *H. erato* comparisons showed recombination rate correlated with divergence, but not admixture. We propose two possible explanations for this difference between the *Heliconius* clades. First, there may be differences in the genetic architecture of the species barriers, such that there are fewer or more tightly clustered barrier loci in the *H. erato* and *H. himera* comparisons, thereby limiting the ability for a correlation between recombination rate and admixture to arise. However, the genetic architectures of adaptive divergence (e.g., color pattern) are strikingly similar in the erato and melpomene clades, and in melpomene, loci responsible for mate preference and adaptive traits (e.g., color pattern) have been demonstrated to be tightly linked (Jiggins et al. 2001; Kronforst et al. 2006; Merrill et al. 2019). Therefore, differences in the number or having too few barrier loci is likely insufficient to explain this difference in admixture patterns between the *H. erato - H. himera* and *H. melpomene – H. cydno/timareta* populations. Alternatively, there may not have been sufficient migration events and time for selection to remove foreign alleles after introgression and thus for a correlation between recombination rate and admixture to arise between *H. erato* and *H. himera*. In this latter case, genetic differences that accumulated in periods of isolation would have had more profound effects on the divergence landscape of *H. erato* and *H. himera* whereas gene flow has likely been more continuous throughout the divergence history of the species pair in the *H. melpomene* clade (Martin et al. 2015b, Martin et al. 2019). These differences in the history of divergence among the co-mimetic species highlights the power of approaches like those applied here to resolve the roles of different evolutionary processes in generating seemingly similar heterogeneous patterns of genomic divergence.

AUTHOR CONTRIBUTIONS

The study was conceived and designed by S.V.B. and B.A.C. in collaboration with R.P. and W.O.M. Genomic analyses were performed by S.V.B. and J.C. Demographic modeling with ∂a∂I was conducted by J.C. Samples of *H. e. cyrbia* from northern Ecuador were contributed by G.M.K., and C.B. assisted with permits. R.P., G.M.K., and W.O.M. provided input on results and manuscript preparation. The manuscript was written and figures were made by SVB, JC, and BAC.

ACKNOWLEDGMENTS

This work was funded by NSF grant (DEB 1257689) to B.A.C. and R.P. and NSF EPSCoR RII Track-2 FEC (OIA 1736026) to R.P. and B.A.C. For sequencing and computational resources, we thank the University of Puerto Rico, the Puerto Rico INBRE Grant P20 GM103475 from the National Institute for General Medical Sciences (NIGMS), a component of the National Institutes of Health (NIH); and awards 1010094 and 1002410 from the EPSCoR program of the NSF. We thank the Ecuadorian Ministerio del Ambiente (No. 005–13 ICFAU- DNB/MA), Peruvian Ministerio de Agricultura and Instituto Nacional de Recursos Naturales (201-2013-MINAGRI-DGFFS/DGEFFSS) and Autoridad Nacional De Licencias Ambientales-ANLA in Colombia (Permiso Marco 0530) for permission to collect butterflies. We thank Simon Martin for sharing his code and useful discussions that shaped this paper. We thank Nicola Nadeau for access to sequence data for northern *H. erato cyrbia* samples, which was funded by her UK Natural Environment Research Council (NERC) fellowship (NE/K008498/1). We thank Matthew Streisfeld and the reviewers for their exceptional help in improving this manuscript.

DATA ARCHIVING

For GenBank accession numbers of whole genome resequence data see Table S1. Scripts and data for RI calculations and genomic analysis are available at https://github.com/StevenVB12/Genomics. Scripts for $\partial a \partial I$ inference are available at https://github.com/jmcole003/2018_herato_demography.

CONFLICT OF INTEREST

The authors have no conflict of interest to declare.

LITERATURE CITED

Aeschbacher, S., J. P. Selby, J. H. Willis, and G. Coop. 2017. Population-genomic inference of the strength and timing of selection against gene flow. Proc. Natl. Acad. Sci 114:7061–7066.

Arias, C. F., S. Van Belleghem, and W. O. McMillan. 2016. Genomics at the evolving species boundary. Curr. Opin. Insect Sci 13:7–15. Elsevier Inc.

Barton, N., and B. O. Bengtsson. 1986. The barrier to genetic exchange between hybridising populations. Heredity (Edinb) 57:357–376.

Barton, N. H., and M. A. R. De Cara. 2009. The evolution of strong reproductive isolation. Evolution 63:1171–1190.

Berner, D., and M. Roesti. 2017. Genomics of adaptive divergence with chromosome-scale heterogeneity in crossover rate. Mol. Ecol 26:6351–6369.

Brandvain, Y., A. M. Kenney, L. Flagel, G. Coop, and A. L. Sweigart. 2014. Speciation and introgression between Mimulus nasutus and Mimulus guttatus. PLoS Genet 10:e1004410.

Browning, B. L., and S. R. Browning. 2016. Genotype imputation with millions of reference samples. Am. J. Hum. Genet. 98:116–126.

Burnham, K. P., and D. R. Anderson. 2004. Multimodel inference: Understanding AIC and BIC in model selection. Sociol. Methods Res 33:261–304.

Burri, R. 2017. Interpreting differentiation landscapes in the light of long-term linked selection. Evol. Lett 1:118–131.

Chan, A. H., P. A. Jenkins, and Y. S. Song. 2012. Genome-wide fine-scale recombination rate variation in *Drosophila melanogaster*. PLoS Genet 8.

Charlesworth, B. 2009. Effective population size and patterns of molecular evolution and variation. Nat. Rev. Genet 10:195–205.

Charlesworth, B. 1998. Measures of divergence between populations and the effect of forces that reduce variability. Mol. Biol. Evol 15:538–543.

Chouteau, M., M. Arias, and M. Joron. 2016. Warning signals are under positive frequency-dependent selection in nature. Proc. Natl. Acad. Sci 113:2164–2169.

Counterman, B. A., F. Araujo-Perez, H. M. Hines, S. W. Baxter, C. M. Morrison, D. P. Lindstrom, R. Papa, L. Ferguson, M. Joron, R. H.

Ffrench-Constant, et al. 2010. Genomic hotspots for adaptation: the population genetics of Müllerian mimicry in *Heliconius erato*. PLoS Genet 6:e1000796.

Crawford, J. E., M. M. Riehle, W. M. Guelbeogo, A. Gneme, N. Sagnon, K. D. Vernick, R. Nielsen, and B. P. Lazzaro. 2015. Reticulate speciation and barriers to introgression in the Anopheles gambiae species complex. Genome Biol. Evol 7:3116–3131.

Cruickshank, T. E., and M. W. Hahn. 2014. Reanalysis suggests that genomic islands of speciation are due to reduced diversity, not reduced gene flow. Mol. Ecol 23:3133–3157.

Dasmahapatra, K. K., J. R. Walters, A. D. Briscoe, J. W. Davey, A. Whibley, N. J. Nadeau, A. V. Zimin, S. Adler, S.-J. Ahn, D. A. Baker, et al. 2012. Butterfly genome reveals promiscuous exchange of mimicry adaptations among species. Nature 487:94–98. Nature Publishing Group.

De Mita, S., and M. Siol. 2012. EggLib: Processing, analysis and simulation tools for population genetics and genomics. BMC Genet 13:27.

Durand, E. Y., N. Patterson, D. Reich, and M. Slatkin. 2011. Testing for ancient admixture between closely related populations. Mol. Biol. Evol 28:2239–2252.

Edelman, N. B., P. B. Frandsen, M. Miyagi, B. Clavijo, J. Davey, R. Dikow, G. García-accinelli, S. M. Van Belleghem, N. Patterson, E. Daniel, et al. 2019. Genomic architecture and introgression shape a butterfly radiation. Science 366:24174–24183.

Ewing, G., and J. Hermisson. 2010. MSMS: a coalescent simulation program including recombination, demographic structure and selection at a single locus. Bioinformatics 26:2064–2065.

Frantz, L. A. F., O. Madsen, H. J. Megens, M. A. M. Groenen, and K. Lohse. 2014. Testing models of speciation from genome sequences: Divergence and asymmetric admixture in Island South-East Asian Sus species during the Plio-Pleistocene climatic fluctuations. Mol. Ecol 23:5566–5574.

Gutenkunst, R. N., R. D. Hernandez, S. H. Williamson, and C. D. Bustamante. 2009. Inferring the joint demographic history of multiple populations from multidimensional SNP frequency data. PLoS Genet 5:e1000695.

Hudson, R. R., M. Slatkin, and W. P. Maddison. 1992. Estimation of levels of gene flow from DNA sequence data. Genetics 132:583–589.

Janousek, V., P. Munclinger, L. Wang, K. C. Teeter, and P. K. Tucker. 2015. Functional Organization of the Genome May Shape the Species Boundary in the House Mouse. Mol. Biol. Evol 2:1208–1220.

Jiggins, C. D., O. Mcmillan, W. Neukirchen, J. Mallet, and L. Nw. 1996. What can hybrid zones tell us about speciation? The case of *Heliconius erato* and *H. himera* (Lepidoptera: Nymphalidae). Biol. J. Linn. Soc 59:221–242.

Jiggins, C. D., R. E. Naisbit, R. L. Coe, and J. Mallet. 2001. Reproductive isolation caused by colour pattern mimicry. Nature 411:302–305.

Kaplan, N. L., R. R. Hudson, and C. H. Langley. 1989. The "hitchhiking effect" revisited. Genetics 123:887–899.

Keinan, A., and D. Reich. 2010. Human population differentiation is strongly correlated with local recombination rate. PLoS Genet 6:e1000886.

Kronforst, M. R., M. E. B. Hansen, N. G. Crawford, J. R. Gallant, W. Zhang, R. J. Kulathinal, D. D. Kapan, and S. P. Mullen. 2013. Hybridization reveals the evolving genomic architecture of speciation. Cell Rep 5:666–677.

Kronforst, M. R., L. G. Young, D. D. Kapan, C. McNeely, R. J. O'Neill, and L. E. Gilbert. 2006. Linkage of butterfly mate preference and wing color preference cue at the genomic location of wingless. Proc. Natl. Acad. Sci. U. S. A 103:6575–6580.

Latour, Y., M. Perriat-Sanguinet, P. Caminade, P. Boursot, C. M. Smadja, and G. Ganem. 2013. Sexual selection against natural hybrids may contribute to reinforcement in a house mouse hybrid zone. Proc. R. Soc. B Biol. Sci 281:20132733.

Lewis, J. J., S. M. Van Belleghem, R. Papa, C. G. Danko, and R. D. Reed. 2020. Many functionally connected loci foster adaptive diversification along a neotropical hybrid zone. Sci. Adv 6:1–11.

Mallet, J. 1986. Hybrid zones of *Heliconius* butterflies in Panama and the stability and movement of warning colour dines. Heredity 56:191–202.

Mallet, J. 1993. Speciation, raciation, and color pattern evolution in *Heliconius* butterflies: evidence from hybrid zones. Pp. 226–260 *in* R. G. Harrison, ed. Hybrid zone and the Evolutionary process. Oxford University Press, New York.

Mallet, J., N. Barton, G. Lamas, J. S. C, M. M. M, and H. Eeley. 1990. Estimates of selection and gene flow from measures of cline width and linkage disequilibrium in *Heliconius* hybrid zones. Genetics 124:921–936.

Mallet, J., and M. Joron. 1999. Evolution of diversity in warning color and mimicry: Polymorphisms, shifting balance and speciation. Annu. Rev. Ecol. Syst 30:201–233.

Martin, S. H., K. K. Dasmahapatra, N. J. Nadeau, C. Salazar, J. R. Walters, F. Simpson, M. Blaxter, A. Manica, J. Mallet, and C. D. Jiggins. 2013. Genome-wide evidence for speciation with gene flow in *Heliconius* butterflies. Genome Res 23:1817–1828.

Martin, S. H., J. W. Davey, and C. D. Jiggins. 2015a. Evaluating the use of ABBA-BABA statistics to locate introgressed loci. Mol. Biol. Evol 32:244–257.

Martin, S. H., J. W. Davey, C. Salazar, and C. D. Jiggins. 2019. Recombination rate variation shapes barriers to introgression across butterfly genomes. PLOS Biol 17:e2006288.

Martin, S. H., A. Eriksson, K. M. Kozak, A. Manica, and C. D. Jiggins. 2015b. Speciation in Heliconius Butterflies : Minimal Contact Followed by Millions of Generations of Hybridisation. BioRxiv 1–24.

Martin, S. H., M. Möst, W. J. Palmer, C. Salazar, W. O. McMillan, F. M. Jiggins, and C. D. Jiggins. 2016. Natural selection and genetic diversity in the butterfly Heliconius melpomene. Genetics 203:525–541.

McMillan, W. O., C. D. Jiggins, and J. Mallet. 1997. What initiates speciation in passion-vine butterflies? Proc. Natl. Acad. Sci. U. S. A 94:8628–8633.

Meier, J. I., P. A. Salazar, M. Ku, R. W. Davies, A. Dréau, I. Aldás, O. B. Power, N. J. Nadeau, J. R. Bridle, C. Rolian, et al. 2020. Haplotype tagging reveals parallel formation of hybrid races in two butterfly species. bioRxiv 1–41.

Merrill, R. M., A. Chia, and N. J. Nadeau. 2014. Divergent warning patterns contribute to assortative mating between incipient *Heliconius* species. Ecol. Evol 4:911–917.

Merrill, R. M., P. Rastas, S. H. Martin, M. C. Melo, S. Barker, J. Davey, W. O. McMillan, and C. D. Jiggins. 2019. Genetic dissection of assortative mating behavior. PLoS Biol 17:e2005902.

Moest, M., S. M. Van Belleghem, J. James, C. Salazar, S. Martin, S. Barker, G. Moreira, C. Mérot, M. Joron, N. Nadeau, et al. 2020. Selective sweeps on novel and introgressed variation shape mimicry loci in a butterfly adaptive radiation. PLoS Biol 18:e3000597.

Muñoz, A. G., C. Salazar, J. Castaño, C. D. Jiggins, and M. Linares. 2010. Multiple sources of reproductive isolation in a bimodal butterfly hybrid zone. J. Evol. Biol 23:1312–1320.

Nachman, M. W., and B. A. Payseur. 2012. Recombination rate variation and speciation: Theoretical predictions and empirical results from rabbits and mice. Philos. Trans. R. Soc. B Biol. Sci 367:409–421.

Nei, M., and W. H. Li. 1979. Mathematical model for studying genetic variation in terms of restriction endonucleases. Proc. Natl. Acad. Sci. U. S. A 76:5269–5273.

Nosil, P., J. L. Feder, S. M. Flaxman, and Z. Gompert. 2017. Tipping points in the dynamics of speciation. Nat. Ecol. Evol 1:1–8.

Pease, J. B., and M. W. Hahn. 2015. Detection and polarization of introgression in a five-taxon phylogeny. Syst. Biol 64:651–662.

Price, A. L., N. J. Patterson, R. M. Plenge, M. E. Weinblatt, N. a Shadick, and D. Reich. 2006. Principal components analysis corrects for stratification in genome-wide association studies. Nat. Genet 38:904–909.

Price, M. N., P. S. Dehal, and A. P. Arkin. 2010. FastTree 2 – Approximately maximum-likelihood trees for large alignments. PLoS One 5:e9490.

Prowell, D. 1998. Sex linkage and speciation in Lepidoptera. Pp. 309–319 *in* D. Howard and S. Berlocher, eds. Endless forms. Species and speciation. Oxford University Press, New York.

Quek, S. P., B. A. Counterman, P. A. De Moura, M. Z. Cardoso, C. R. Marshall, W. O. McMillan, and M. R. Kronforst. 2010. Dissecting comimetic radiations in *Heliconius* reveals divergent histories of convergent butterflies. Proc. Natl. Acad. Sci. U. S. A 107:7365–7370.

Ravinet, M., R. Faria, R. K. Butlin, J. Galindo, N. Bierne, M. Rafajlovic, M. A. F. Noor, B. Mehlig, and A. M. Westram. 2017. Interpreting the genomic landscape of speciation: a road map for finding barriers to gene flow. J. Evol. Biol 30:1450–1477.

Reed, R. D., R. Papa, A. Martin, H. M. Hinas, B. A. Counterman, C. Pardo-Diaz, C. D. Jiggins, N. L. Chamberlain, M. R. Kronforst, R. Chen, et al. 2011. *optix* drives the repeated convergent evolution of butterfly wing pattern mimicry. Science 333:1137–1141.

Rougeux, C., L. Bernatchez, and P. A. Gagnaire. 2017. Modeling the multiple facets of speciation-with-gene-flow toward inferring the divergence history of lake whitefish species pairs (*Coregonus clupeaformis*). Genome Biol. Evol 9:2057–2074.

Roux, C., C. Fraisse, J. Romiguier, Y. Anciaux, N. Galtier, and N. Bierne. 2016. Shedding light on the grey zone of speciation along a continuum of genomic divergence. PLoS Biol 14:e2000234.

Schumer, M., C. Xu, D. L. Powell, A. Durvasula, L. Skov, C. Holland, J. C. Blazier, and S. Sankararaman. 2018. Natural selection interacts with recombination to shape the evolution of hybrid genomes. Science (80-.). 660:656–660.

Shaak, S. G. 2015. Selection dynamics in *Heliconius* hybrid zones and the origin of adaptive variation. Mississippi State University.

Sobel, J. M., and G. F. Chen. 2014. Unification of methods for estimating the strength of reproductive isolation. Evolution (N. Y) 68:1511–1522.

Sperling, F. A. H. 1994. Sex-linked genes and species differences in Lepidoptera. Can. Entomol 126:807–818.

Stankowski, S., M. A. Chase, A. M. Fuiten, M. F. Rodrigues, P. L. Ralph, and M. A. Streisfeld. 2019. Widespread selection and gene flow shape the genomic landscape during a radiation of monkeyflowers. PLOS Biol 17:e3000391.

Supple, M., R. Papa, H. M. Hines, W. O. McMillan, and B. A. Counterman. 2015. Divergence with gene flow across a speciation continuum of *Heliconius* butterflies. BMC Evol. Biol 15:204.

Tavares, H., A. Whibley, D. L. Field, D. Bradley, M. Couchman, L. Copsey, J. Elleouet, M. Burrus, C. Andalo, M. Li, et al. 2018. Selection and gene flow shape genomic islands that control floral guides. Proc. Natl. Acad. Sci. U. S. A 115:11006–11011.

Tine, M., H. Kuhl, P. A. Gagnaire, B. Louro, E. Desmarais, R. S. T. Martins, J. Hecht, F. Knaust, K. Belkhir, S. Klages, et al. 2014. European sea bass genome and its variation provide insights into adaptation to euryhalinity and speciation. Nat. Commun 5:5770.

Van Belleghem, S. M., P. Rastas, A. Papanicolaou, S. H. Martin, C. F. Arias, M. A. Supple, J. J. Hanly, J. Mallet, J. J. Lewis, H. M. Hines, et al. 2017. Complex modular architecture around a simple toolkit of wing pattern genes. Nat. Ecol. Evol 1:52.

Van Belleghem, S. M., C. Salazar, C. D. Jiggins, M. Baquero, R. Papa, B. A. Counterman, W. O. Mcmillan, and S. H. Martin. 2018. Patterns of Z chromosome divergence among *Heliconius* species highlight the importance of historical demography. Mol. Ecol 27:3852–3872.

Wallbank, R. W. R., S. W. Baxter, C. Pardo-diaz, J. Hanly, S. H. Martin, J. Mallet, and K. K. Dasmahapatra. 2016. Evolutionary novelty in a butterfly wing pattern through enhancer shuffling. PLoS Biol 14:e1002353.

Wolf, J. B. W., and H. Ellegren. 2017. Making sense of genomic islands of differentiation in light of speciation. Nat. Rev. Genet 18:87–100.

Wu, C. 2001. The genic view of the process of speciation. J. Evol. Biol 14:851–865.

Associate Editor: M. Streisfeld
Handling Editor: A. McAdam

Supporting Information

Additional supporting information may be found online in the Supporting Information section at the end of the article.

Table S1. Samples used in this study. Samples from *H. himera* populations and *H. erato* populations that come into contact with *H. himera* are indicated in color. *H. himera* North, light red; *H. himera* South, dark red; *H. e. cyrbia* North, light yellow, *H. e. cyrbia* South, dark yellow; *H. e. emma* East, light green; *H. e. emma* West dark green; *H. e. favorinus* East, light blue; *H. e. favorinus* West, dark blue. Earthcape IDs are available through https://heliconius.ecdb.io.

Table S2. Hybrid zone characteristics between *H. erato* and *H. himera* populations. Major color pattern (CP) loci include the genes *optix* (∼red), *WntA* (∼forewing band shape) and *cortex* (∼yellow hindwing bar and white fringes) Reproductive isolation (*RI*) was estimated as a combination of ecological isolation (RI_{ec}) due to divergent selection on color patterns, pre-mating isolation (RI_{pre}) due to mate preference, and post-mating isolation (RI_{post}) due to hybrid sterility.

Table S3. 2D *δaδi* model descriptions.

Table S4. Bash pseudocode to run *msms* (Ewing and Hermisson 2010) simulations. Note that mutation rate is only used by *seq-gen* when simulating the sequences, population size is used to scale times, selection and migration proportions.

Table S5. AIC weights dadi models. AIC scores for each model are averages of the top 5 runs. Shaded cells indicate lowest AIC values.

Table S6. Best model parameters for best model class as well as alternative model classes. Split times are given as Ttotal+TAM in AM, and Ttotal+TSC in SC. Although all best fitting demographic models include secondary contact (SC), several alternative models including AM (Ancient Migration) and IM (Isolation and Migration) fit relatively well to the observed JSFS (Figure 3A; Figure S4-5). However, in these models, migration rates generally scale proportionately with migration duration compared to the SC models, indicating that our interpretations on migration rates should not be affected by the uncertainty of finding a best demographic model.

Figure S1. FastTree of samples used in this study. Node support values are based on the Shimodaira–Hasegawa test.

Figure S2. Average AIC (Akaike Information Criterion) of all tested $\delta a \delta i$ models for twenty runs. SI = Strict Isolation, IM = Isolation and Migration, AM = Ancestral Migration, SC = Secondary Contact, G = exponential growth, 2N = heterogeneous effective population size (with 2 classes of loci shared by the two populations = Hill-Robertson effects), and 2m = 2 migration rates.

Figure S3. Average AIC (Akaike Information Criterion) of all tested $\delta a \delta i$ models for twenty runs using subpopulations. SI = Strict Isolation, IM = Isolation and Migration, AM = Ancestral Migration, SC = Secondary Contact, G = exponential growth, 2N = heterogeneous effective population size (with 2 classes of loci shared by the two populations = Hill-Robertson effects), and 2m = 2 migration rates.

Figure S4. Inference of historical effective population size changes using pairwise sequentially Markovian coalescent (PSMC) analysis. Lines and shading in the left panel represent the average effective population size and 95% CI, respectively, estimated from PSMC analyses on individual genome samples as shown in the panels on the right. The PSMC estimates are scaled using a generation time of 0.25 years and a mutation rate of 2e-9. Data adopted from Van Belleghem et al. (2018).

Figure S5. Loess fit to admixture (f_d) between *H. himera* and *H. erato* in three contact zones. Points show admixture (fd) values, whereas coloring shows directionality (DFOIL) in 50 kb non-overlapping windows for the contact zones *H. himera* ¬– *H. e. cyrbia* (top), *H. himera – H. e. emma* (middle) and *H. himera – H. e. favorinus* (bottom) as in Figure 3. Blue indicates predominant admixture from *H. erato* into *H. himera* (12 ← 34), whereas red indicates predominant admixture from *H. himera* into *H. erato* (12 → 34) based on the DFOIL tests. Green lines indicate the Loess fit.

Figure S6. Comparison of admixture (f_d) signals with relative divergence (d_a) of single *H. erato* individuals to *H. himera*. Panels with black points show the f_d signals between contact zones of *H. himera* with *H. e. cyrbia* (top), *H. e. emma* (middle) and *H. e. favorinus (bottom)*. Panels with colored points show relative divergence d_a, calculated from pairwise sequence differences minus the average nucleotide diversity of both populations, between *H. himera* and a single individual of a hybridizing *H. erato* population. Green rectangles are high f_d tracks as identified from a Loess fit to continues windows of f_d larger than 0.06 for the *H. e. cyrbia* and *H. e. emma* contact zones and 0.07 for the *H. e. favorinus* contact zone.

Figure S7. Correlations of divergence and admixture proportions with recombination rate and gene density in *H. himera – H. erato* contact zones. (A) Relative divergence (F_{ST}) versus gene density and recombination rate (ρ). (B) Admixture proportion (f_d) versus gene density and recombination rate (cM/Mb). (C) Relative divergence (F_{ST}) versus admixture proportion (f_d). Statistics were calculated in 50 kb non-overlapping windows. Colored circles match color codes in Figure 2.

Figure S8. Expected relationship of recombination rate with divergence (F_{ST}) and admixture (f_d) near a divergently selected locus ($s = 0.02$). (A) The population tree shows the simulated scenario with the onset of divergent selection on a derived allele indicated in red and in which migration rate (m) and migration time (t_m) between P2 and P3 and selection start time (t_s) are varied. Left and right of the simulated scenario are parameter combinations for two extreme scenarios that both include linked selection; on the left a scenario with Isolation with Migration (IM) and on the right a scenario reflecting Secondary Contact (SC). **(B)** Effect of population recombination rate (ρ) on relative divergence (F_{ST}) and admixture (f_d) near a divergently selected locus for the two simulated scenarios with parameter combinations as in panel A. The selected allele occurs at position 0. The dashed red line indicates a locus at 500 kb from the selected locus at which the relationship between ρ, divergence and admixture is assessed in panel C. **(C)** The effect of migration start time (t_m) and selection start time (t_s) on the relation between ρ, divergence and admixture. Apart from the respective parameters being evaluated, other parameters were fixed as in panel A, with the red lines indicating the exact parameter combinations as in panel A and B.